

# MambaVO: Deep Visual Odometry Based on Sequential Matching Refinement and Training Smoothing

Shuo Wang<sup>1\*</sup>, Wanting Li<sup>1\*</sup>, Yongcai Wang<sup>1†</sup>, Zhaoxin Fan<sup>2,3†</sup>,  
Zhe Huang<sup>1</sup>, Xudong Cai<sup>1</sup>, Jian Zhao<sup>4,5</sup>, Deying Li<sup>1</sup>

<sup>1</sup>School of Information, Renmin University of China

<sup>2</sup>Beijing Advanced Innovation Center for Future Blockchain and Privacy Computing,  
Institute of Artificial Intelligence, Beihang University

<sup>3</sup>Hangzhou International Innovation Institute, Beihang University

<sup>4</sup>The Institute of AI (TeleAI), China Telecom

<sup>5</sup>School of Artificial Intelligence, Optics and Electronics (iOPEN),  
Northwestern Polytechnical University (NWPU), Xi'an China

\*Equal contribution    †Corresponding authors

## Abstract

*Deep visual odometry has demonstrated great advancements by learning-to-optimize technology. This approach heavily relies on the visual matching across frames. However, ambiguous matching in challenging scenarios leads to significant errors in geometric modeling and bundle adjustment optimization, which undermines the accuracy and robustness of pose estimation. To address this challenge, this paper proposes MambaVO, which conducts robust initialization, Mamba-based sequential matching refinement, and smoothed training to enhance the matching quality and improve the pose estimation. Specifically, the new frame is matched with the closest keyframe in the maintained Point-Frame Graph (PFG) via the semi-dense based Geometric Initialization Module (GIM). Then the initialized PFG is processed by a proposed Geometric Mamba Module (GMM), which exploits the matching features to refine the overall inter-frame matching. The refined PFG is finally processed by differentiable BA to optimize the poses and the map. To deal with the gradient variance, a Trending-Aware Penalty (TAP) is proposed to smooth training and enhance convergence and stability. A loop closure module is finally applied to enable MambaVO++. On public benchmarks, MambaVO and MambaVO++ demonstrate SOTA performance, while ensuring real-time running.*

## 1. Introduction

Visual Odometry (VO) is the task of tracking an agent’s six-DOF poses when interacting with the physical world, which

is critical for robots, self-driving cars and other autonomous agents [23, 54, 55]. Early works mainly rely on geometric feature methods [3, 38, 41], in which, the frontend extracts feature points and conducts feature matching [31, 43, 60], while the backend optimizes poses and build maps using filtering [16] or optimization methods [9, 27, 56]. However, the geometric features are less effective in challenging environments, such as scenes with weak textures.

Building on the progress in computer vision and deep learning, early approaches have explored using neural networks to directly regress poses [30, 35, 45, 53]. However, these methods suffer from poor accuracy and lack generalization to unseen environments. A more promising paradigm is the concept of *learning to optimize* [47, 49, 51], where neural networks are utilized to extract features and perform matching, while differentiable nonlinear optimization layers [40, 47] refine poses based on geometric residuals. This type of method has achieved state-of-the-art results in the field of deep visual odometry [34, 51].

The success of learning-to-optimize deep VO lies on the nested optimization of the sequential image matching network and the differentiable Bundle Adjustment (BA). Although being successful, we find that the accuracy and robustness of matching and pose optimization in existing methods are limited by three key aspects. (1) **Unstable initialization**. Existing methods using random patches [51], predicted optical flow [49], or motion prediction [25] may fail to provide robust initial estimates in challenging environments. (2) **Less refined matching**. Accurate inter-frame correspondences are crucial for visual odometry. Current feature extraction and limited feature interaction restrict the

matching precision [34, 51]. (3) **The training challenges:** The gradient variance problem is a main challenge for the nested optimization in learning to optimize, which causes instability and slow convergence [21]. While some methods adjust the loss via gradient weighting [21], this can lead to overfitting, limiting generalization to unseen environments.

To tackle the issue, we propose MambaVO, a novel VO system that refines inter-frame image matching and produces more accurate and robust poses using a Mamba-based module. MambaVO introduces three key components. First, a Point-Frame Graph (PFG) captures observation relationships, enabling robust initialization and sequence-based matching refinement. Second, the Geometric Initialization Module (GIM) uses semi-dense matching [59] and PnP [28, 64] to predict pixel correspondences and initialize poses, extracting features for fusion in subsequent matching refinement. Third, the Geometric Mamba Module (GMM) refines pixel matches by leveraging historical tokens and fusion features through Mamba blocks, adjusting pixel correspondences and frame weights within the PFG. To ensure stable training, we further introduce the Trending-Aware Penalty (TAP), which balances pose and matching losses, addressing gradient variance issues [21]. We also extend MambaVO to MambaVO++, incorporating loop closure for global optimization in SLAM.

Our contributions are summarized as follows:

- We propose a novel VO system, MambaVO, designed to address Unstable initialization, less refined matching, and training challenges in deep VO methods.
- We introduce three key components to enhance MambaVO: (1) the Geometric Initialization Module (GIM), which ensures robust pose initialization using semi-dense matching and PnP; (2) the Geometric Mamba Module (GMM), which refines pixel correspondences using historical tokens and fusion features; and (3) the Trending-Aware Penalty (TAP), which stabilizes training by balancing pose and matching losses.
- We extend the system to MambaVO++, incorporating loop closure for global optimization in a full SLAM system. Through extensive experiments on EuRoC [1], TUM-RGBD [46], KITTI [15], and TartanAir [57], MambaVO and MambaVO++ achieve state-of-the-art performance in accuracy, while ensuring real-time performance and lower GPU memory consumption compared to recent learning-to-optimize methods.

## 2. Related Work

Traditional visual odometry and SLAM methods have produced numerous notable approaches, including direct methods like DSO [14], SVO [12], and LSD-SLAM [11], as well as feature-based methods such as ORB-SLAM [38], VINS-Mono [41], and OpenVINS [16]. However, we focus on deep visual odometry, which forms the core of our study.

### 2.1. Direct Pose Regression for Visual Odometry

Early deep visual odometry methods, which we refer to as direct pose regression approaches, applied neural networks to predict relative poses from visual inputs [6, 35, 53]. DeepVO [35] was one of the first works to use CNNs to predict rotation and translation changes from sequential images. VINet [6] and VidLoc [5] framed visual-inertial odometry as a sequence-to-sequence learning problem. In unsupervised learning, methods aimed to estimate depth and pose without labeled data. SfM-Learner [65] used photometric consistency to predict both pose and depth. Although it outperformed traditional methods like ORB-SLAM [38] (without loop closure), it still struggled with generalization. SfM-Net [52] took this further by jointly estimating optical flow, scene flow, and 3D point clouds. Un-DeepVO [30] used stereo images during training to address the scale ambiguity in monocular VO, improving accuracy.

While these methods demonstrated promising results, they often exhibited limitations in accuracy and generalization across diverse environments. Therefore, this paper explores a more stable learning-to-optimize approach.

### 2.2. Learning to Optimize for Visual Odometry

The Learning to Optimize approach has gained prominence with the adoption of differentiable bundle adjustment [40, 47]. Early works, such as BA-Net [47], introduced a bundle adjustment layer to optimize photometric re-projection error. Some other methods refined pose estimates via geometric constraints predicted by neural networks [7, 24] and learned correspondence weights to improve optimization [36, 42]. DROID-SLAM [49] improved upon this by refining per-pixel depth using advanced optical flow, overcoming the limitations of basis depth maps, and employing dense bundle adjustment to further enhance accuracy. DPVO [51] introduced patch tracking with refinement, leading to more efficient pose estimation while reducing computational costs. Its follow-up work, DPV-SLAM [34], extended global optimization by leveraging a patch-graph structure. More recently, V2V [21] identified training challenges caused by gradient variances and mitigated the issue by dynamically weighting the loss.

While these approaches have advanced visual odometry performance, they suffer from less refined matching and inaccuracy poses in low-texture or repetitive environments. In this paper, we propose MambaVO to tackle the issues.

### 2.3. State Space Models

State Space Models (SSMs) [19, 20] have garnered significant attention due to their ability to capture long-range dependencies with linear complexity, making them highly effective across a variety of fields. A recent advancement in SSMs, the Mamba architecture [18], introduces a selection mechanism to extract features from sequential data more

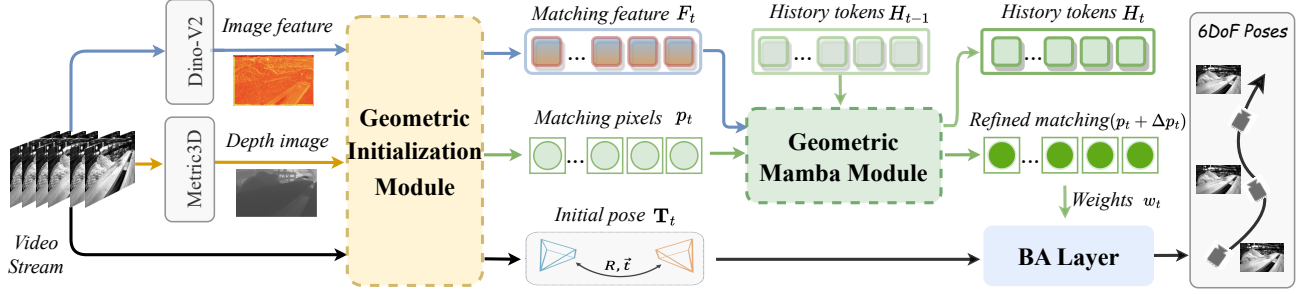


Figure 1. The proposed MambaVO extracts Dino-v2[39] features from the input RGB sequence and estimates the depth[22] for keyframes. In the Geometric Initialization Module (Sec. 3.1), a semi-dense matching network is utilized to generate initial matches, estimate the initial poses, and extract features for each match. Next, the Geometric Mamba Module(Sec. 3.2) refines and re-weights the matching. Finally, we use a differentiable bundle adjustment (BA) to optimize the final poses, ensuring accuracy and stability in the pose estimation process.

efficiently. Mamba has achieved outstanding results in diverse applications. Vision Mamba [66] enhances visual representation by scanning the visual space for better feature extraction. VideoMamba [29] efficiently processes video patches to learn temporal information. In collaborative perception, Mamba fuses spatial features from multiple agents [32], highlighting its versatility in multi-agent systems.

In our work, we model VO as a task of refining image matching and poses across sequences. Leveraging Mamba blocks with semi-dense initialization, we enhance the ability to fuse and refine matching across frames, thereby significantly improving accuracy and robustness. To the best of our knowledge, this is the first time SSMs have been employed in the context of visual odometry.

### 3. Methods

The overview of MambaVO is shown in Fig. 1. Given a sequence of RGB images as input, MambaVO solves the set of camera poses  $\{\mathbf{T}_\tau\}_{\tau=0}^N$  and the reconstructed map points  $\{P_i\}_{i=0}^L$ , where  $\mathbf{T}_\tau \in SE(3)$  represents the camera pose of frame  $\tau$ , and  $P_i = (x_i, y_i, z_i)^\top$  denotes the position of map point  $i$  in the world coordinate system.

We model the observation relationship between the map points and the cameras, as well as the frame co-visibility, using a *Point-Frame Graph (PFG)*  $\mathcal{G} = (\mathcal{V}, \mathcal{E})$ . The PFG vertices represent camera poses and map points. The edge between camera frames (frame-frame edge), such as  $(t-1, t)$  represents the pose transformation  $\mathbf{T}_{t-1, t}$  between them. Frame-point edges represent projections. An edge  $(i, t) \in \mathcal{E}$  indicates the camera observes the map point  $i$  in the  $t$ -th frame. We define the observed pixel coordinates as  $p_t^i = (u_t^i, v_t^i)^\top$ . The projection relationship for edge  $(i, t)$  is described using the projection function:

$$p_t^i = \Pi(\mathbf{T}_t, P_i) = \mathbf{K}\mathbf{T}_t P_i \quad (1)$$

where  $\mathbf{K}$  is the intrinsic matrix of the camera. If both edges  $(i, t-1)$  and  $(i, t)$  exist, it means that the same map point

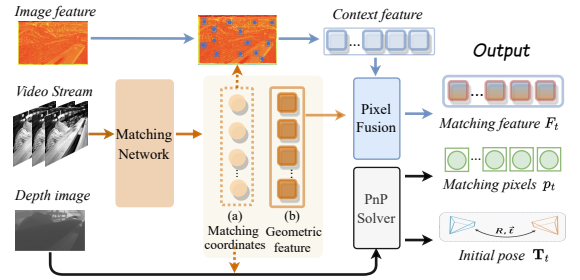


Figure 2. Illustration of Geometric Initialization Module. GIM extracts geometric and context features, and performs matching using a semi-dense matching network. The initial pose is estimated using a PnP solver based on the matched pixels.

is observed in both the  $t-1$  frame and the  $t$  frame. This co-visibility and association is initialized by image matching in the initialization step (Sec. 3.1). To minimize computational costs, we maintain only the latest PFG within a sliding window containing  $\mathcal{W}$  frames. The PFG is initialized from the first frame pair.

#### 3.1. Geometric Initialization Module: GIM

##### 3.1.1. Matching and Pose Initialization.

After receiving the  $t$ -th image, the nearest keyframe  $r$  in time order in PFG serves as the reference frame for initial matching and feature extraction. We utilize Dino-v2 [39] to extract context features, and EfficientLoFTR [59] provides  $k$  initially matched coordinates  $\{[p_r^i, p_t^i]\}_{i=1}^k$  and pixel-wise geometric features  $\mathbf{G}_t = \{\mathbf{G}_t^i\}_{i=1}^k$  from the fine-matching module in EfficientLoFTR. These  $k$  matches are used to estimate the initial pose  $\mathbf{T}_t$  of the frame  $t$ . We apply Metric3D [22] to estimate the depth for each matched point in the reference frame, denoted by  $\{d_r^i\}_{i=1}^k$ . By obtaining the 3D points and by the 3D-2D correspondences, PnP (Perspective-n-Point) [28] calculates the initial pose  $\mathbf{T}_t$  and

refine the 3D coordinates of the matched points:

$$\begin{aligned} \mathbf{T}_{r,t}, \{\mathbf{P}_i\}_{i=1}^k &= \text{PnP}(\{[p_r^i, p_t^i]\}_{i=1}^k, \{d_r^i\}_{i=1}^k) \\ \mathbf{T}_t &= \mathbf{T}_{r,t} \mathbf{T}_r \end{aligned} \quad (2)$$

where  $\mathbf{T}_{r,t}$  is the relative pose between frame  $r$  and  $t$ .

### 3.1.2. Matching Feature Preparation

As in Fig. 2, we prepare matching features for matching refinement by the Geometric Mamba Module (Sec. 3.2). The matched pixels in frame  $i$  are used to query the context features from Divo-v2 encoder, yielding the pixel-wise context features  $\mathbf{C}_t = \{\mathbf{C}_t^i\}_{i=1}^k$ . Context features  $\mathbf{C}_t$  and geometric features  $\mathbf{G}_t$  are fused via concatenation, 1D convolution, and ReLU activation to obtain the fused matching feature  $\mathbf{F}_t^i$  for each matched pixel in the pixel fusion process:

$$\mathbf{F}_t^i = \text{ReLU}(\text{1DConv}(\text{Concat}(\mathbf{G}_t^i, \mathbf{C}_t^i))), i \in [1, k] \quad (4)$$

where  $\mathbf{F}_t^i \in \mathbb{R}^{1 \times 384}$ .  $\mathbf{F}_t \in \mathbb{R}^{k \times 384}$  represents all matching features in the current frame  $t$ . The initialized PFG will then be processed by the Geometric Mamba Module.

## 3.2. Geometric Mamba Module: GMM

GMM refines the matching coordinates of each frame at the pixel level by sequentially learning the matching features in PFG. It accepts the PFG as input, including the matching points  $\{[p_r^i, p_t^i]\}_{i=1}^k$  for each frame pair and the corresponding matching features  $\mathbf{F}_t$ . Using these matching features and the history tokens, GMM refines the matching coordinates and estimates the matching weights. GMM consists of two main parts: History Fusion and Geometric Mamba Blocks. The detailed structure is in Fig. 3.

### 3.2.1. History Fusion

Odometry is essentially a time series problem, and historical information affects current inter-frame matching through sequential pose transformation and overlapping areas. We maintain the history token  $H_{t-1} \in \mathbb{R}^{k \times 384}$  to represent the historical information and fuse with  $\mathbf{F}_t$  in History Fusion. The history token for the first frame is initialized from the matching features in GIM. Specifically, we perform cross-attention between  $\mathbf{F}_t^i$  and  $H_{t-1}$  on each edge in PFG:

$$\hat{M}_t^i = \text{CrossAttention}(\mathbf{F}_t^i, H_{t-1}), i \in [1, k] \quad (5)$$

Then, we concatenate all  $\hat{M}_t^i$  of the current frame and perform linear mapping on the edge dimension to conduct 1D convolution:

$$\{M_t^i\}_{i=1}^k = \text{Conv1D}(\text{Concat}(\{\hat{M}_t^i\}_{i=1}^k)) \quad (6)$$

We then repack  $\{M_t^i\}_{i=1}^k$  to  $\mathbf{M}_t \in \mathbb{R}^{k \times 384}$  to represent the *matching tokens* of all the  $k$  edges related to the current frame  $t$ , which are used in the subsequent Mamba blocks. This matching feature and history combination design can effectively integrate history information, providing stronger consistency and stability for the final feature expression.

### 3.2.2. Geometric Mamba Blocks

Geometric Mamba Blocks contains  $B$  vanilla Mamba blocks[18], receiving the historical token  $H_{t-1}$  along with all the matching tokens  $\{\mathbf{M}_\tau\}_{\tau=t-\mathcal{W}}^t$  from PFG, where the number of vertices is  $\mathcal{W} + 1$ . Geometric Mamba Blocks output an updated history token  $\hat{H}_t$  and the refined matching tokens  $\{\mathbf{M}_\tau\}_{\tau=t-\mathcal{W}}^t$  for PFG.

$$\hat{H}_t, \{\mathbf{M}_\tau\}_{\tau=t-\mathcal{W}}^t = \text{MambaBlocks}(H_{t-1}, \{\mathbf{M}_\tau\}_{\tau=t-\mathcal{W}}^t) \quad (7)$$

Each updated matching token  $M_\tau^i \in \mathbf{M}_\tau$  is further decoded by a Matching Refinement Head, i.e. RefineHead(). For the edge  $(i, \tau)$  in PFG and the corresponding matching token  $M_\tau^i$ , the Matching Refinement Head outputs the pixel refinement  $\Delta p_\tau^i$  and the matching weights  $w_\tau^i$  respectively, which are subsequently used to update the edge  $(i, \tau)$  and the pixel coordinates  $p_\tau^i$ .

$$\begin{aligned} \Delta p_\tau^i, w_\tau^i &= \text{RefineHead}(M_\tau^i) \\ \tau &\in [t - \mathcal{W}, t], i \in [1, k] \end{aligned} \quad (8)$$

where  $\Delta p_\tau^i \in \mathbb{R}^2$  and  $w_\tau^i \in \mathbb{R}^2$  represent the adjusted pixels and the weight for the matching. RefineHead() contains two MLPs for decoding  $\Delta p_\tau^i$  and  $w_\tau^i$  respectively. The updated token  $\hat{H}_t$  is then combined with  $H_{t-1}$  from the previous time step through a GRU module to generate the new history token  $H_t$ .

$$H_t = \text{GRU}(\hat{H}_t, H_{t-1}) \quad (9)$$

From above process, it can be seen that GMM takes the result of GIM as input and continuously refines and reweights the matching in all the frame vertices in the PFG. With the refinement and evaluated weight for each matching, the cameras' poses and map points are updated through the differentiable bundle adjustment layer[50]. The predicted  $\Delta p_\tau$  and  $w_\tau$  are engaged in the objective function.

$$\mathbf{T}, \mathbf{P} = \arg \min_{\mathbf{T}, \mathbf{P}} \sum_{(i, \tau) \in \mathcal{E}} \|\Pi(\mathbf{T}_\tau, \mathbf{P}_i) - (p_\tau^i + \Delta p_\tau^i)\|_{w_\tau^i} \quad (10)$$

where  $\|\cdot\|_{w_\tau^i}$  is the Mahalanobis distance weighted by  $w_\tau^i$ . We employ the Gauss-Newton method in the BA layer[50] to linearize the objective, update the poses and map points while keeping the matching constant, ensuring that the induced trajectory adjustments are consistent with the predicted matching updates.

## 3.3. Smoothed Training

During training, we jointly train GIM and GMM with the BA layer, an implicit nonlinear optimization module. However, nested optimization causes loss oscillations and convergence challenges. To address this, we introduce the Trending-Aware Penalty to stabilize the loss and improve convergence.

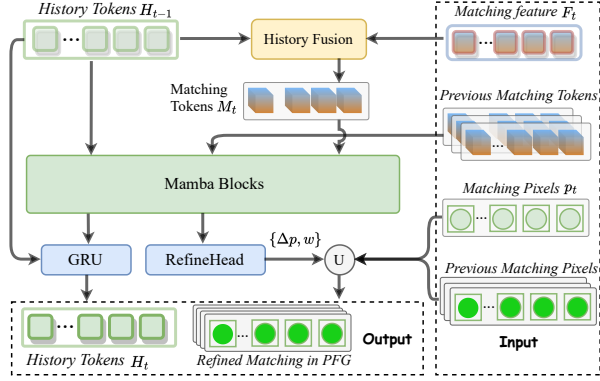


Figure 3. Illustration of Geometric Mamba Module. The GIM refines the matching by incorporating both current and historical information. Matching tokens  $M_t$  are derived from matching features and previous matching tokens, then processed through Mamba blocks. The RefineHead further decodes the refinement and the weight for each matching.

### 3.3.1. Training Loss

We apply supervision to the poses and the matching as in [49, 51]. In training, we randomly select a set of trajectory segments and each works as a training sample, whose camera poses and the matching ground truth are used as the supervision signal. The PFG for an arbitrary training sample is denoted as  $\mathcal{G} = (\mathcal{V}, \mathcal{E})$ . The final predicted poses are compared with the ground truth poses to compute the relative error loss between each two frames in  $\mathcal{V}$ :

$$\mathcal{L}_{pose} = \sum_{\tau_1, \tau_2 \in \mathcal{V}} \|\text{Log}_{SE(3)} \left[ (\tilde{\mathbf{T}}_{\tau_1}^{-1} \tilde{\mathbf{T}}_{\tau_2})^{-1} (\mathbf{T}_{\tau_1}^{-1} \mathbf{T}_{\tau_2}) \right] \|\quad (11)$$

where  $\tilde{\mathbf{T}}$  is the ground truth and  $\mathbf{T}$  is the predicted pose.

We also supervise the estimated matching pixels and the ground truth. The weights from GMM are used to weight the loss, to focus on the matching pixels that are more important for pose estimation.

$$\hat{\mathcal{L}}_{match} = \sum_{(i, \tau) \in \mathcal{E}} \|\tilde{p}_{\tau}^i - p_{\tau}^i\|_{w_{\tau}^i} \quad (12)$$

where  $p_{\tau}^i$  is the predicted matching coordinates, and  $\tilde{p}_{\tau}^i$  is the ground truth.

### 3.3.2. Trending-Aware Penalty

The gradient of the loss exhibits significant fluctuations due to the variance of trajectories (e.g., motion patterns, lighting, textures), as reported in [21, 51], and is also seen in our experiments (Fig. 5). Further, there are differences in the learning speed of the pose loss and the matching loss. These lead to negative impacts on the training convergence.

We propose a **Trending-Aware Penalty (TAP)** to solve the above training challenges. We first calculate the *gradient weighting parameter* as in [21], which evaluates the

gradient difference of the pose loss and the matching loss. We adjust the matching loss by the gradient weighting parameter every 50 training iterations to balance the pose loss gradient and the matching loss gradient.

$$\mathcal{L}_{match} = \frac{\|\nabla_{\theta} \mathcal{L}_{pose}\|_2}{\|\nabla_{\theta} \mathcal{L}_{match}\|_2} \hat{\mathcal{L}}_{match} \quad (13)$$

Considering the variance brought by different trajectories, we further propose a *trend-based balance parameter* by averaging the losses over historical training iterations. For the  $t$ -th training iteration,  $\Lambda_{match}$  evaluates the decreasing trend of matching loss by comparing with the average loss of the past four iterations.

$$\Lambda_{match} = \exp \left( \frac{\mathcal{L}_{match}^t}{\frac{1}{4} \sum_{k=0}^3 \mathcal{L}_{match}^{t-k}} \right) \quad (14)$$

We get  $\Lambda_{pose}$  in the same way and obtain the trend-based balance parameter, i.e.,  $\Lambda = \frac{\Lambda_{match}}{\Lambda_{pose}}$ .  $\Lambda$  measures the trend difference. Finally, the total loss is balanced by the trend difference to emphasize the one that decreases more slowly.

$$\mathcal{L} = \mathcal{L}_{pose} + \Lambda \mathcal{L}_{match} \quad (15)$$

## 4. MambaVO and MambaVO++

We implement a complete visual odometry system, **MambaVO**, based on the proposed network modules. The system takes RGB sequence as input and performs real-time camera tracking and map reconstruction. To ensure high efficiency and accuracy, we adopt a keyframe strategy. To correct the accumulated drift, we further develop **MambaVO++**, which is a SLAM system incorporating loop closure and global optimization to enhance the overall performance.

**Keyframes and Optimization.** A frame is selected as a keyframe if it meets either of the two conditions: (1) the parallax with the previous frame exceeds 30px, or (2) none of the last three frames are keyframes. We maintain a sliding window of keyframes ( $\mathcal{W}$  is set to 10 in our experiments).

**Loop Closure and Global Optimization.** We use a DBoW2-based loop closure strategy [3]. We extract ORB features from keyframes and store all key frames to maintain the global pose graph. DBoW2 [13] performs place recognition to retrieve loop closure pairs. For loop closure pairs, we calculate the relative pose using matching and the PnP in Sec. 3.1. Based on the loop closure edges, we run a global optimization to correct the accumulated drift. These processes are completed in parallel on the CPU.

## 5. Experiments

We evaluate MambaVO and MambaVO++ on four datasets: EuRoC [1], TUM-RGBD [46], KITTI [15], and TartanAir

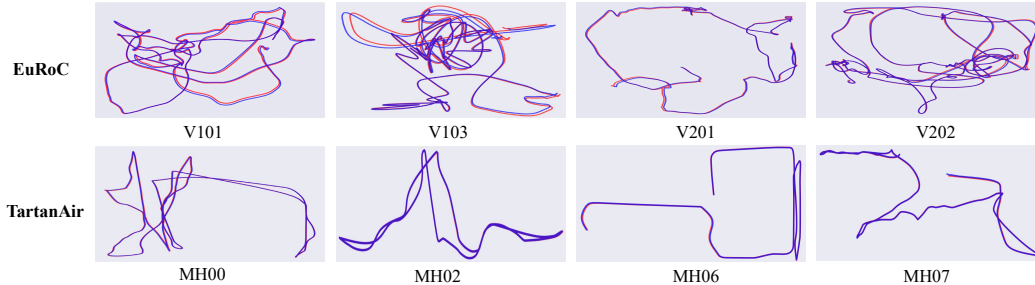


Figure 4. Qualitative visualization. The blue line represents the trajectory estimated by MambaVO, and the red line represents the ground truth. The results show that our estimated trajectory almost completely coincides with the ground truth.

[57]. Our model is trained only on the TartanAir training set, without retraining or fine-tuning on other datasets, which is the same as [21, 49, 51]. We train our network for 196k steps with a batch size of 1. Training takes 2.5 days on one RTX 4090 GPU.

### 5.1. Analysis on Pose Estimation

We report pose estimation results on the TartanAir test-split from the CVPR 2020 SLAM competition in Tab. 1, EuRoC in Tab. 2, KITTI in Tab. 3, and TUM-RGBD in Tab. 4. We run evaluations five times and report the mean ATE (Absolute Trajectory Error) results from the EVO tool [17] under a monocular setting only. We separate methods that without and with loop closure to ensure a fair comparison with MambaVO and MambaVO++ respectively. The qualitative results are shown in Fig. 4.

As the results in Tab. 1-Tab. 4, our method performs robustly across all scenarios, while previous methods fail on certain sequences (marked “X”). Our Methods achieve the SOTA results (on AVG column) in both loop closure settings. Notably, MambaVO reduces the pose estimation error by 19%-22% on average comparing to DROID-VO [49], DPVO [51], and V2V [21] on indoor datasets like EuRoC, TUM-RGBD, and TartanAir.

We can also observe that loop closure and global optimization significantly enhance localization accuracy. In particular, on long sequences like KITTI and EuRoC, MambaVO++ achieves over 50% improvement compared to MambaVO, demonstrating the benefits of traditional loop closure and global optimization.

### 5.2. Analysis on Matching Improvement

Method	AUC@1 $^\uparrow$	AUC@2 $^\uparrow$	AUC@5 $^\uparrow$	AUC@10 $^\uparrow$
DROID-VO[49]	0.123	0.167	0.294	0.53
DPVO[51]	0.299	0.485	0.738	0.925
V2V[21]	<u>0.399</u>	<u>0.584</u>	<u>0.855</u>	<u>0.957</u>
MambaVO (Ours)	<b>0.471</b>	<b>0.678</b>	<b>0.892</b>	<b>0.975</b>

Table 5. Geometric matching experiments on EuRoC dataset. The top one is in **bold** and the second is underlined.

To further evaluate how the Mamba architecture contributes to the matching improvement, we evaluate the image matching metric separately. The compared methods include other visual odometry algorithms. Disabling bundle adjustment and optimization, we use only the matching outputs to compute relative poses between frames via Poselib [28], which employs epipolar error [63] and LO-RANSAC [4]. Poses are evaluated using the AUC (Area Under the Curve) metric, following the image matching methods in [2, 59].

As in Tab. 5, MambaVO achieves the best matching performance compared with previous methods on EuRoC dataset. DROID-VO relying on the dense flow matching, often introduces noise in correspondences in challenging areas. DPVO and V2V samples pixel patches and perform matching by inner product on image feature, resulting in poor fine-matching capability. Our GMM enhances pixel-level matching accuracy, especially improving AUC@1 $^\circ$  and AUC@2 $^\circ$  by 17% and 16%, respectively, over the previous best. This highlights the effectiveness of our geometric initialization and Mamba-based sequential refinement.

### 5.3. Ablation Study

We conduct ablation studies to study the impacts of different components and different design choices.

#### 5.3.1. Impact of Feature Selection in GIM

Feature Selection	SIFT[33]	ORB[43]	SP[10]	Patch[51]	Ours
TartanAir	4.29	5.07	2.35	<u>0.18</u>	<b>0.14</b>
EuRoC	0.524	1.184	1.758	<u>0.115</u>	<b>0.094</b>

Table 6. Ablation experiments on matching feature. We report the ATE[m] $\downarrow$  results on EuRoC dataset. The top one is in **bold** and the second is underlined.

In GIM, we used the geometric feature of EfficientLoFTR, i.e.  $\mathbf{G}_t$  for matching. We replace the feature matching by SIFT [33], ORB [43], Superpoint [10], and random patches [51] respectively to perform ablation experiments on the EuRoC dataset to figure out how the matching feature affects the deep visual odometry. The results are shown in

	Method	MH000	MH001	MH002	MH003	MH004	MH005	MH006	MH007	AVG
w. loop	ORBSLAM3[3]	15.44	2.92	13.51	8.18	2.59	21.91	11.70	25.88	14.38
	COLMAP[44]	12.26	13.45	13.45	20.95	24.97	16.79	7.01	7.97	12.5
	DeFlowSLAM[61]	0.63	0.06	<b>0.02</b>	<b>0.01</b>	2.8	0.20	0.31	0.45	0.56
	DROID-SLAM[49]	<b>0.08</b>	<u>0.05</u>	<u>0.04</u>	<u>0.02</u>	<b>0.01</b>	0.68	0.30	<u>0.07</u>	0.33
	DPV-SLAM[34]	0.23	<u>0.05</u>	<u>0.04</u>	0.04	0.54	<u>0.15</u>	<u>0.07</u>	0.14	<u>0.16</u>
	MambaVO++(Ours)	<u>0.12</u>	<b>0.04</b>	<b>0.02</b>	<u>0.02</u>	<u>0.37</u>	<b>0.14</b>	<b>0.05</b>	<b>0.05</b>	<b>0.10</b>
w.o. loop	TartanVO[58]	4.88	0.26	2.00	0.94	1.07	3.19	1.00	2.04	1.92
	DROID-VO[49]	0.32	0.13	0.08	0.09	1.52	0.69	0.39	0.97	0.58
	DPVO[51]	<u>0.21</u>	0.04	<u>0.04</u>	<u>0.08</u>	<u>0.58</u>	<b>0.17</b>	<u>0.11</u>	<u>0.15</u>	<u>0.17</u>
	V2V[21]	0.18	<u>0.03</u>	<b>0.03</b>	<b>0.02</b>	<u>0.58</u>	0.30	<b>0.08</b>	<b>0.05</b>	0.18
	MambaVO (Ours)	0.24	<b>0.02</b>	<b>0.03</b>	<b>0.02</b>	<b>0.46</b>	<u>0.18</u>	0.13	<b>0.05</b>	<b>0.14</b>

Table 1. ATE[m] $\downarrow$  results on the TartanAir test split. The top one is in **bold** and the second is underlined.

	Method	MH01	MH02	MH03	MH04	MH05	V101	V102	V103	V201	V202	V203	AVG
w. loop	ORBSLAM3[3]	0.016	0.027	0.028	0.138	0.072	<b>0.033</b>	0.015	0.033	0.023	0.029	$\times$	-
	LDSO[14]	0.046	0.035	0.175	1.954	0.385	0.093	0.085	-	0.043	0.405	-	-
	GO-SLAM[62]	0.016	<b>0.014</b>	0.023	<u>0.045</u>	0.045	0.037	<u>0.011</u>	0.023	0.016	0.010	0.022	0.024
	DROID-SLAM[49]	<u>0.013</u>	<b>0.014</b>	<u>0.022</u>	<b>0.043</b>	0.043	0.037	0.012	0.02	<u>0.017</u>	<u>0.013</u>	<b>0.014</b>	<u>0.022</u>
	DPV-SLAM[34]	<u>0.013</u>	<u>0.016</u>	<u>0.022</u>	<b>0.043</b>	<u>0.041</u>	<u>0.035</u>	<b>0.008</b>	<b>0.015</b>	0.020	<b>0.011</b>	0.040	0.024
	MambaVO++(Ours)	<b>0.012</b>	0.017	<b>0.020</b>	<b>0.043</b>	<b>0.035</b>	<u>0.035</u>	<b>0.008</b>	0.016	<b>0.016</b>	0.015	<u>0.018</u>	<b>0.021</b>
w.o. loop	DeepV2D[48]	1.614	1.492	1.635	1.775	<b>1.013</b>	0.717	0.695	1.483	0.839	1.052	0.591	1.173
	TartanVO[58]	<u>0.639</u>	0.325	0.550	1.153	<u>1.021</u>	0.447	0.389	0.622	<u>0.433</u>	0.749	1.152	0.680
	SVO[12]	0.10	0.12	0.41	0.43	0.30	0.07	0.21	$\times$	0.11	0.11	1.08	-
	DROID-VO[49]	0.163	0.121	0.242	0.399	0.270	0.103	0.165	0.158	0.102	0.115	<u>0.204</u>	0.186
	DPVO[51]	0.087	0.055	<u>0.158</u>	<b>0.137</b>	0.114	0.050	<u>0.140</u>	<b>0.086</b>	0.057	<u>0.049</u>	0.211	<u>0.105</u>
	V2V[21]	0.081	0.067	0.171	0.179	0.115	<u>0.046</u>	0.16	<u>0.097</u>	0.056	0.059	0.252	0.117
	MambaVO(Ours)	<b>0.063</b>	<b>0.024</b>	<b>0.107</b>	<u>0.148</u>	0.118	<b>0.044</b>	<b>0.138</b>	0.1	<b>0.035</b>	<b>0.047</b>	<b>0.208</b>	<b>0.094</b>

Table 2. ATE[m] $\downarrow$  results on the EuRoC. The top one is in **bold** and the second is underlined.

Tab. 6. We demonstrate the obvious ATE decreasing in using our semi-dense feature.

### 5.3.2. Impact of Modules in GIM, GMM and TAP

The ablation study results presented in Tab. 7 provide the impacts of components in the GIM, GMM, and TAP. The experiments are conducted on the EuRoC and KITTI and we report the ATE metric. When evaluating GIM’s components, we fix the GMM and TAP, and vice visa.

The results indicate that in GIM, both the context features and geometric features significantly contribute to reducing ATE. PnP is crucial for accuracy, especially on the KITTI outdoor dataset, where the localization error rises significantly without the initial poses of PnP. For GMM, removing any key component degrades performance. In particular, removing the Mamba blocks causes the failure on KITTI. In addition, our TAP strategy during training contributes to the accuracy in unseen scenarios like EuRoC and KITTI. The full MambaVO achieves the best performance with all the components.

### 5.3.3. Impact of Smoothed Training Loss

We evaluate the two parameters for training loss smoothing (Sec. 3.3), one is the gradient weighting parameter and the other is the trend-based balance parameter. We retrained MambaVO without the either kind of the parameter and re-

port the ATE on the TartanAir validation set. The results are shown in Fig. 5. We can observe that with the assistance of these two parameters, the loss curve converges faster and more stably. It also achieves lower ARE on the validation set under the same training iterations.

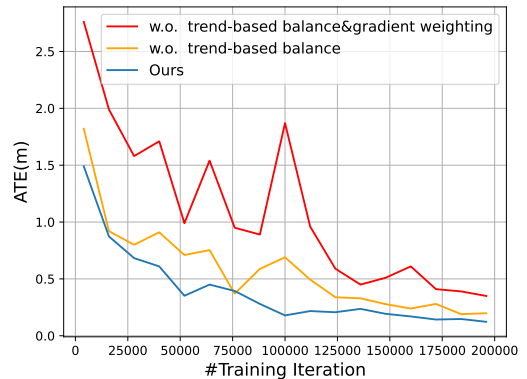


Figure 5. We report the average ATE on the validation split of TartanAir. We observe that our loss design strategy makes training converge faster and achieve smaller ATE error.

	Method	00	01	02	03	04	05	06	07	08	09	10	AVG
w. loop	ORB-SLAM2[37]	8.27	<b>X</b>	<b>26.86</b>	1.21	<u>0.77</u>	7.91	12.54	3.44	<b>46.81</b>	76.54	<b>6.61</b>	-
	ORB-SLAM3[3]	<u>6.77</u>	<b>X</b>	30.50	<b>1.036</b>	0.93	5.542	16.605	9.70	<u>60.69</u>	<b>7.89</b>	<u>8.65</u>	-
	LDSO[14]	9.32	11.68	31.98	2.85	1.22	<u>5.1</u>	13.55	2.96	129.02	<u>21.64</u>	17.36	<u>22.42</u>
	DROID-SLAM[49]	92.1	344.6	<b>X</b>	2.38	1.00	118.5	62.47	21.78	161.60	<b>X</b>	118.70	-
	DPV-SLAM[34]	112.80	<u>11.50</u>	123.53	2.50	0.81	57.8	54.86	18.77	110.49	76.66	13.65	53.03
	DPV-SLAM++[34]	8.30	11.86	39.64	2.50	0.78	5.74	<b>11.6</b>	<b>1.52</b>	110.9	76.70	13.70	25.76
	MambaVO++(Ours)	<b>6.19</b>	<b>8.04</b>	<u>27.73</u>	1.94	<b>0.59</b>	<b>3.05</b>	<u>11.79</u>	<u>1.7</u>	105.42	63.24	10.51	<b>21.84</b>
w.o. loop	DROID-VO[49]	<b>98.43</b>	84.20	<u>108.8</u>	2.58	0.93	59.27	64.4	24.20	<b>64.55</b>	<b>71.8</b>	16.91	54.19
	DPVO[51]	113.21	<u>12.69</u>	123.4	<u>2.09</u>	<u>0.68</u>	<u>58.96</u>	<b>54.78</b>	19.26	<u>115.90</u>	75.10	<b>13.63</b>	<u>53.03</u>
	MambaVO(Ours)	<u>112.39</u>	<b>8.16</b>	<b>93.78</b>	<b>1.80</b>	<b>0.66</b>	<b>56.51</b>	<u>57.19</u>	<b>17.9</b>	116.01	<u>73.56</u>	<u>14.37</u>	<b>50.21</b>

Table 3. ATE[m] $\downarrow$  results on the KITTI dataset. The top one is in **bold** and the second is underlined.

	Method	360	desk	desk2	floor	plant	room	rpy	teddy	xyz	AVG
w. loop	ORB-SLAM2[37]	<b>X</b>	0.071	<b>X</b>	0.023	<b>X</b>	<b>X</b>	<b>X</b>	<b>X</b>	0.01	-
	ORB-SLAM3[3]	<b>X</b>	<u>0.017</u>	<b>0.21</b>	<b>X</b>	0.034	<b>X</b>	<b>X</b>	<b>X</b>	<b>0.009</b>	-
	GO-SLAM[62]	<u>0.089</u>	<b>0.016</b>	<u>0.028</u>	<u>0.025</u>	0.026	<u>0.052</u>	<b>0.019</b>	<u>0.048</u>	<u>0.01</u>	<u>0.035</u>
	DROID-SLAM[49]	0.111	0.018	0.042	<b>0.021</b>	<b>0.016</b>	<b>0.049</b>	<u>0.026</u>	<u>0.048</u>	0.012	0.038
	DPV-SLAM[34]	0.112	0.018	0.029	0.057	<u>0.021</u>	0.33	0.03	0.084	<u>0.01</u>	0.076
	MambaVO++(Ours)	<b>0.085</b>	<b>0.016</b>	0.032	0.027	0.025	0.056	<u>0.026</u>	<b>0.029</b>	<b>0.009</b>	<b>0.034</b>
w.o. loop	TartanVO[58]	0.178	0.125	0.122	<u>0.349</u>	0.297	<b>0.333</b>	0.049	0.339	0.062	0.206
	DeepV2D[48]	0.182	0.652	0.633	0.579	0.582	0.776	0.053	0.602	0.15	0.468
	DeepFactors[8]	0.159	0.17	0.253	0.169	0.305	<u>0.364</u>	0.043	0.601	0.035	0.233
	DPVO[51]	<u>0.135</u>	0.038	0.048	0.04	0.036	0.394	<u>0.034</u>	0.064	<b>0.012</b>	<u>0.089</u>
	V2V[21]	0.145	<u>0.026</u>	<u>0.044</u>	0.064	<u>0.031</u>	0.434	0.045	<b>0.046</b>	<b>0.012</b>	0.094
	MambaVO(Ours)	<b>0.108</b>	<b>0.021</b>	<b>0.037</b>	<b>0.034</b>	<b>0.022</b>	0.372	<b>0.031</b>	<u>0.048</u>	<u>0.013</u>	<b>0.076</b>

Table 4. ATE[m] $\downarrow$  results on the TUM-RGBD dataset. We only conduct experiments under the monocular setting. The top one is in **bold** and the second is underlined.

	Configuration	EuRoC	KITTI
GIM	w.o. Context feature	0.181	58.62
	w.o. Geometric feature	0.309	192.75
	w.o. PnP	0.199	201.16
GMM	w.o. History fusion	0.179	59.97
	w.o. Mamba blocks	0.318	<b>X</b>
	w.o. GRU	0.293	190.01
TAP	w.o. Gradient weight	0.111	50.87
	w.o. History balance	0.101	51.93
	MambaVO (full)	<b>0.094</b>	<b>50.21</b>

Table 7. Ablation experiments on modules in MambaVO. We report the ATE[m] $\downarrow$  results. The top one is in **bold**.

## 5.4. Time and Memory

MambaVO can run in real-time on a single RTX 3090 GPU. On EuRoC, we achieve an average real-time performance of 22Hz, exceeding the camera frame rate of 20Hz. On the TUM-RGBD and KITTI datasets, the frame rates are 30Hz and 23Hz, respectively. All of the results are obtained under the settings shown in the Tab. 2, Tab. 3, Tab. 4.

We also compared GPU memory usage for inference with current state-of-the-art deep visual odometry methods. Experimental results demonstrate that our method has smaller GPU memory consumption during inference, as the

results shown in Fig. 6.

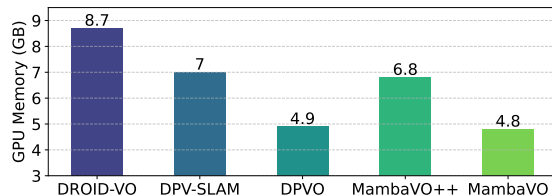


Figure 6. GPU memory usage of MambaVO and MambaVO++ compared to other methods.

## 6. Conclusion

This paper proposes MambaVO, a novel deep visual odometry system to address the accuracy and robustness of deep VO based on learning to optimize. We conduct reliable initialization, sequential matching refinement, and training smoothing based on the Mamba architecture. Our method achieves the state-of-the-art results on TartanAir, EuRoC, TUM-RGBD, and KITTI. In the future, we will utilize dense information and 3D Gaussian Splatting [26] technology to obtain high-fidelity maps for rich scene representation while maintaining localization accuracy.

## References

- [1] Michael Burri, Janosch Nikolic, Pascal Gohl, Thomas Schneider, Joern Rehder, Sammy Omari, Markus W Achtelik, and Roland Siegwart. The euroc micro aerial vehicle datasets. *The International Journal of Robotics Research*, 35(10):1157–1163, 2016. 2, 5
- [2] Xudong Cai, Yongcai Wang, Lun Luo, Minhang Wang, Deying Li, Jintao Xu, Weihao Gu, and Rui Ai. Prism: Progressive dependency maximization for scale-invariant image matching. *arXiv preprint arXiv:2408.03598*, 2024. 6
- [3] Carlos Campos, Richard Elvira, Juan J Gómez Rodríguez, José MM Montiel, and Juan D Tardós. Orb-slam3: An accurate open-source library for visual, visual-inertial, and multi-map slam. *IEEE Transactions on Robotics*, 37(6):1874–1890, 2021. 1, 5, 7, 8
- [4] Ondřej Chum, Jiří Matas, and Josef Kittler. Locally optimized ransac. In *Pattern Recognition: 25th DAGM Symposium, Magdeburg, Germany, September 10-12, 2003. Proceedings 25*, pages 236–243. Springer, 2003. 6
- [5] Ronald Clark, Sen Wang, Andrew Markham, Niki Trigoni, and Hongkai Wen. Vidloc: A deep spatio-temporal model for 6-dof video-clip relocalization. In *Proceedings of the IEEE conference on computer vision and pattern recognition*, pages 6856–6864, 2017. 2
- [6] Ronald Clark, Sen Wang, Hongkai Wen, Andrew Markham, and Niki Trigoni. Vinet: Visual-inertial odometry as a sequence-to-sequence learning problem. In *Proceedings of the AAAI conference on artificial intelligence*, 2017. 2
- [7] Ronald Clark, Michael Bloesch, Jan Czarnowski, Stefan Leutenegger, and Andrew J Davison. Learning to solve non-linear least squares for monocular stereo. In *Proceedings of the European Conference on Computer Vision (ECCV)*, pages 284–299, 2018. 2
- [8] Jan Czarnowski, Tristan Laidlow, Ronald Clark, and Andrew J Davison. Deepfactors: Real-time probabilistic dense monocular slam. *IEEE Robotics and Automation Letters*, 5(2):721–728, 2020. 8
- [9] Frank Dellaert. Factor graphs and gtsam: A hands-on introduction. *Georgia Institute of Technology, Tech. Rep.*, 2:4, 2012. 1
- [10] Daniel DeTone, Tomasz Malisiewicz, and Andrew Rabinovich. Superpoint: Self-supervised interest point detection and description. In *Proceedings of the IEEE conference on computer vision and pattern recognition workshops*, pages 224–236, 2018. 6
- [11] Jakob Engel, Thomas Schöps, and Daniel Cremers. Lsdslam: Large-scale direct monocular slam. In *European conference on computer vision*, pages 834–849. Springer, 2014. 2
- [12] Christian Forster, Matia Pizzoli, and Davide Scaramuzza. Svo: Fast semi-direct monocular visual odometry. In *2014 IEEE international conference on robotics and automation (ICRA)*, pages 15–22. IEEE, 2014. 2, 7
- [13] Dorian Gálvez-López and J. D. Tardós. Bags of binary words for fast place recognition in image sequences. *IEEE Transactions on Robotics*, 28(5):1188–1197, 2012. 5
- [14] Xiang Gao, Rui Wang, Nikolaus Demmel, and Daniel Cremers. Ldso: Direct sparse odometry with loop closure. In *2018 IEEE/RSJ International Conference on Intelligent Robots and Systems (IROS)*, pages 2198–2204. IEEE, 2018. 2, 7, 8
- [15] Andreas Geiger, Philip Lenz, and Raquel Urtasun. Are we ready for autonomous driving? the kitti vision benchmark suite. In *2012 IEEE conference on computer vision and pattern recognition*, pages 3354–3361. IEEE, 2012. 2, 5
- [16] Patrick Geneva, Kevin Eickenhoff, Woosik Lee, Yulin Yang, and Guoquan Huang. Opencvins: A research platform for visual-inertial estimation. In *2020 IEEE International Conference on Robotics and Automation (ICRA)*, pages 4666–4672. IEEE, 2020. 1, 2
- [17] Michael Grupp. evo: Python package for the evaluation of odometry and slam. <https://github.com/MichaelGrupp/evo>, 2017. 6
- [18] Albert Gu and Tri Dao. Mamba: Linear-time sequence modeling with selective state spaces. *arXiv preprint arXiv:2312.00752*, 2023. 2, 4
- [19] Albert Gu, Karan Goel, and Christopher Ré. Efficiently modeling long sequences with structured state spaces. *arXiv preprint arXiv:2111.00396*, 2021. 2
- [20] Albert Gu, Karan Goel, Ankit Gupta, and Christopher Ré. On the parameterization and initialization of diagonal state space models. *Advances in Neural Information Processing Systems*, 35:35971–35983, 2022. 2
- [21] Swaminathan Gurumurthy, Karnik Ram, Bingqing Chen, Zachary Manchester, and Zico Kolter. From variance to veracity: Unbundling and mitigating gradient variance in differentiable bundle adjustment layers. In *Proceedings of the IEEE/CVF Conference on Computer Vision and Pattern Recognition*, pages 27507–27516, 2024. 2, 5, 6, 7, 8
- [22] Mu Hu, Wei Yin, Chi Zhang, Zhipeng Cai, Xiaoxiao Long, Hao Chen, Kaixuan Wang, Gang Yu, Chunhua Shen, and Shaojie Shen. Metric3d v2: A versatile monocular geometric foundation model for zero-shot metric depth and surface normal estimation. *arXiv preprint arXiv:2404.15506*, 2024. 3
- [23] Zhe Huang, Shuo Wang, Yongcai Wang, Wanting Li, Deying Li, and Lei Wang. Roco: Robust cooperative perception by iterative object matching and pose adjustment. In *Proceedings of the 32nd ACM International Conference on Multimedia*, pages 7833–7842, 2024. 1
- [24] Krishna Murthy Jatavallabhula, Ganesh Iyer, and Liam Paull. Dense slam meets automatic differentiation. In *2020 IEEE International Conference on Robotics and Automation (ICRA)*, pages 2130–2137. IEEE, 2020. 2
- [25] Nikhil Keetha, Jay Karhade, Krishna Murthy Jatavallabhula, Gengshan Yang, Sebastian Scherer, Deva Ramanan, and Jonathon Luiten. Splatam: Splat track & map 3d gaussians for dense rgb-d slam. In *Proceedings of the IEEE/CVF Conference on Computer Vision and Pattern Recognition*, pages 21357–21366, 2024. 1
- [26] Bernhard Kerbl, Georgios Kopanas, Thomas Leimkühler, and George Drettakis. 3d gaussian splatting for real-time radiance field rendering. *ACM Trans. Graph.*, 42(4):139–1, 2023. 8

- [27] Rainer Kümmerle, Giorgio Grisetti, Hauke Strasdat, Kurt Konolige, and Wolfram Burgard. g2o: A general framework for graph optimization. In *2011 IEEE international conference on robotics and automation*, pages 3607–3613. IEEE, 2011. 1
- [28] Viktor Larsson and contributors. PoseLib - Minimal Solvers for Camera Pose Estimation, 2020. 2, 3, 6
- [29] Kunchang Li, Xinhao Li, Yi Wang, Yinan He, Yali Wang, Limin Wang, and Yu Qiao. Videomamba: State space model for efficient video understanding. *arXiv preprint arXiv:2403.06977*, 2024. 3
- [30] Ruihao Li, Sen Wang, Zhiqiang Long, and Dongbing Gu. Undeepvo: Monocular visual odometry through unsupervised deep learning. In *2018 IEEE international conference on robotics and automation (ICRA)*, pages 7286–7291. IEEE, 2018. 1, 2
- [31] Wanting Li, Yongcai Wang, Yongyu Guo, Shuo Wang, Yu Shao, Xuewei Bai, Xudong Cai, Qiang Ye, and Deying Li. Colslam: A versatile collaborative slam system for mobile phones using point-line features and map caching. In *Proceedings of the 31st ACM International Conference on Multimedia*, pages 9032–9041, 2023. 1
- [32] Yang Li, Quan Yuan, Guiyang Luo, Xiaoyuan Fu, Xuanhan Zhu, Yujia Yang, Rui Pan, and Jinglin Li. Colmamba: Efficient collaborative perception with cross-agent spatial-temporal state space model. *arXiv preprint arXiv:2409.07714*, 2024. 3
- [33] Tony Lindeberg. Scale invariant feature transform. 2012. 6
- [34] Lahav Lipson, Zachary Teed, and Jia Deng. Deep Patch Visual SLAM. In *European Conference on Computer Vision*, 2024. 1, 2, 7, 8
- [35] Vikram Mohanty, Shubh Agrawal, Shaswat Datta, Arna Ghosh, Vishnu Dutt Sharma, and Debashish Chakravarty. Deepvo: A deep learning approach for monocular visual odometry. *arXiv preprint arXiv:1611.06069*, 2016. 1, 2
- [36] Dominik Muhle, Lukas Koestler, Krishna Murthy Jatavallabhula, and Daniel Cremers. Learning correspondence uncertainty via differentiable nonlinear least squares. In *Proceedings of the IEEE/CVF Conference on Computer Vision and Pattern Recognition*, pages 13102–13112, 2023. 2
- [37] Raul Mur-Artal and Juan D Tardós. Orb-slam2: An open-source slam system for monocular, stereo, and rgb-d cameras. *IEEE transactions on robotics*, 33(5):1255–1262, 2017. 8
- [38] Raul Mur-Artal, Jose Maria Martinez Montiel, and Juan D Tardos. Orb-slam: a versatile and accurate monocular slam system. *IEEE transactions on robotics*, 31(5):1147–1163, 2015. 1, 2
- [39] Maxime Oquab, Timothée Darcet, Théo Moutakanni, Huy Vo, Marc Szafraniec, Vasil Khalidov, Pierre Fernandez, Daniel Haziza, Francisco Massa, Alaaeldin El-Nouby, et al. Dinov2: Learning robust visual features without supervision. *arXiv preprint arXiv:2304.07193*, 2023. 3
- [40] Luis Pineda, Taosha Fan, Maurizio Monge, Shobha Venkataraman, Paloma Sodhi, Ricky TQ Chen, Joseph Ortiz, Daniel DeTone, Austin Wang, Stuart Anderson, Jing Dong, Brandon Amos, and Mustafa Mukadam. Theseus: A Library for Differentiable Nonlinear Optimization. *Advances in Neural Information Processing Systems*, 2022. 1, 2
- [41] Tong Qin, Peiliang Li, and Shaojie Shen. Vins-mono: A robust and versatile monocular visual-inertial state estimator. *IEEE transactions on robotics*, 34(4):1004–1020, 2018. 1, 2
- [42] René Ranftl and Vladlen Koltun. Deep fundamental matrix estimation. In *Proceedings of the European conference on computer vision (ECCV)*, pages 284–299, 2018. 2
- [43] Ethan Rublee, Vincent Rabaud, Kurt Konolige, and Gary Bradski. Orb: An efficient alternative to sift or surf. In *2011 International conference on computer vision*, pages 2564–2571. Ieee, 2011. 1, 6
- [44] Johannes Lutz Schönberger and Jan-Michael Frahm. Structure-from-motion revisited. In *Conference on Computer Vision and Pattern Recognition (CVPR)*, 2016. 7
- [45] Shihao Shen, Yilin Cai, Wenshan Wang, and Sebastian Scherer. Dytanvo: Joint refinement of visual odometry and motion segmentation in dynamic environments. In *2023 IEEE International Conference on Robotics and Automation (ICRA)*, pages 4048–4055. IEEE, 2023. 1
- [46] J. Sturm, N. Engelhard, F. Endres, W. Burgard, and D. Cremers. A benchmark for the evaluation of rgb-d slam systems. In *Proc. of the International Conference on Intelligent Robot Systems (IROS)*, 2012. 2, 5
- [47] Chengzhou Tang and Ping Tan. Ba-net: Dense bundle adjustment network. *arXiv preprint arXiv:1806.04807*, 2018. 1, 2
- [48] Zachary Teed and Jia Deng. Deepv2d: Video to depth with differentiable structure from motion. *arXiv preprint arXiv:1812.04605*, 2018. 7, 8
- [49] Zachary Teed and Jia Deng. Droid-slam: Deep visual slam for monocular, stereo, and rgb-d cameras. *Advances in neural information processing systems*, 34:16558–16569, 2021. 1, 2, 5, 6, 7, 8
- [50] Zachary Teed and Jia Deng. Tangent space backpropagation for 3d transformation groups. In *Proceedings of the IEEE/CVF Conference on Computer Vision and Pattern Recognition (CVPR)*, 2021. 4
- [51] Zachary Teed, Lahav Lipson, and Jia Deng. Deep patch visual odometry. *Advances in Neural Information Processing Systems*, 36, 2024. 1, 2, 5, 6, 7, 8
- [52] Sudheendra Vijayanarasimhan, Susanna Ricco, Cordelia Schmid, Rahul Sukthankar, and Katerina Fragkiadaki. Sfnet: Learning of structure and motion from video. *arXiv preprint arXiv:1704.07804*, 2017. 2
- [53] Sen Wang, Ronald Clark, Hongkai Wen, and Niki Trigoni. Deepvo: Towards end-to-end visual odometry with deep recurrent convolutional neural networks. In *2017 IEEE international conference on robotics and automation (ICRA)*, pages 2043–2050. IEEE, 2017. 1, 2
- [54] Shuo Wang, Yongcai Wang, Xuewei Bai, and Deying Li. Communication efficient, distributed relative state estimation in uav networks. *IEEE journal on selected areas in communications*, 41(4):1151–1166, 2023. 1
- [55] Shuo Wang, Yongcai Wang, Deying Li, and Qianchuan Zhao. Distributed relative localization algorithms for multi-robot networks: A survey. *Sensors*, 23(5):2399, 2023. 1

- [56] Shuo Wang, Yongcai Wang, Zhimin Xu, Yongyu Guo, Wanting Li, Zhe Huang, Xuewei Bai, and Deying Li. Gslamot: A tracklet and query graph-based simultaneous locating, mapping, and multiple object tracking system. In *Proceedings of the 32nd ACM International Conference on Multimedia*, pages 7239–7248, 2024. [1](#)
- [57] Wenshan Wang, Delong Zhu, Xiangwei Wang, Yaoyu Hu, Yuheng Qiu, Chen Wang, Yafei Hu, Ashish Kapoor, and Sebastian Scherer. Tartanair: A dataset to push the limits of visual slam. In *2020 IEEE/RSJ International Conference on Intelligent Robots and Systems (IROS)*, pages 4909–4916. IEEE, 2020. [2](#), [6](#)
- [58] Wenshan Wang, Yaoyu Hu, and Sebastian Scherer. Tartanvo: A generalizable learning-based vo. In *Conference on Robot Learning*, pages 1761–1772. PMLR, 2021. [7](#), [8](#)
- [59] Yifan Wang, Xingyi He, Sida Peng, Dongli Tan, and Xiaowei Zhou. Efficient loftr: Semi-dense local feature matching with sparse-like speed. In *Proceedings of the IEEE/CVF Conference on Computer Vision and Pattern Recognition*, pages 21666–21675, 2024. [2](#), [3](#), [6](#)
- [60] Shichao Yang, Yu Song, Michael Kaess, and Sebastian Scherer. Pop-up slam: Semantic monocular plane slam for low-texture environments. In *2016 IEEE/RSJ International Conference on Intelligent Robots and Systems (IROS)*, pages 1222–1229. IEEE, 2016. [1](#)
- [61] Weicai Ye, Xingyuan Yu, Xinyue Lan, Yuhang Ming, Jinyu Li, Hujun Bao, Zhaopeng Cui, and Guofeng Zhang. Deflow slam: Self-supervised scene motion decomposition for dynamic dense slam. *arXiv preprint arXiv:2207.08794*, 2022. [7](#)
- [62] Youmin Zhang, Fabio Tosi, Stefano Mattoccia, and Matteo Poggi. Go-slam: Global optimization for consistent 3d instant reconstruction. In *Proceedings of the IEEE/CVF International Conference on Computer Vision*, pages 3727–3737, 2023. [7](#), [8](#)
- [63] Zhengyou Zhang. Determining the epipolar geometry and its uncertainty: A review. *International journal of computer vision*, 27:161–195, 1998. [6](#)
- [64] Yinqiang Zheng, Yubin Kuang, Shigeki Sugimoto, Kalle Astrom, and Masatoshi Okutomi. Revisiting the pnp problem: A fast, general and optimal solution. In *Proceedings of the IEEE International Conference on Computer Vision*, pages 2344–2351, 2013. [2](#)
- [65] Tinghui Zhou, Matthew Brown, Noah Snavely, and David G Lowe. Unsupervised learning of depth and ego-motion from video. In *Proceedings of the IEEE conference on computer vision and pattern recognition*, pages 1851–1858, 2017. [2](#)
- [66] Lianghai Zhu, Bencheng Liao, Qian Zhang, Xinlong Wang, Wenyu Liu, and Xinggang Wang. Vision mamba: Efficient visual representation learning with bidirectional state space model. *arXiv preprint arXiv:2401.09417*, 2024. [3](#)